Journal of Power Sources 329 (2016) 104–114

Contents lists available at ScienceDirect

Journal of Power Sources

journal homepage: www.elsevier.com/locate/jpowsour

Facile fabrication of ultrathin hybrid membrane for highly flexible supercapacitors via in-situ phase separation of polyethersulfone

Xiaoning Zhao [a], Fen Ran [a, b, *], Kuiwen Shen [a], Yunlong Yang [a], Jiayu Wu [a], Xiaoqin Niu [b], Lingbin Kong [a], Long Kang [a], Shaowei Chen [b, **]

[a] State Key Laboratory of Advanced Processing and Recycling of Non-ferrous Metals, Lanzhou University of Technology, Lanzhou, 730050, PR China
[b] Department of Chemistry and Biochemistry, University of California, 1156 High Street, Santa Cruz, CA, 95064, USA

HIGHLIGHTS

- A flexible electrode membrane was synthesized via in-situ phase separation method.
- Hierarchical porous structure provided space for migration of electrolyte ions.
- A high specific capacitance was obtained along with long-term cycle life.

GRAPHICAL ABSTRACT

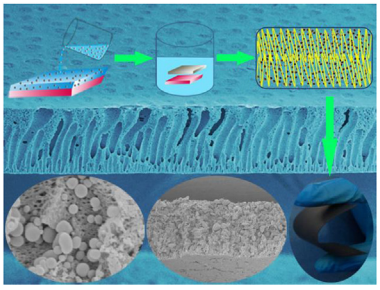

ARTICLE INFO

Article history:
Received 6 April 2016
Received in revised form
16 July 2016
Accepted 9 August 2016

Keywords:
Flexible electrodes
Hybrid membrane
Phase separation
Supercapacitors

ABSTRACT

In this article, a facile method based on in-situ phase-separation was developed for the fabrication of ultrathin hybrid membranes for highly flexible supercapacitors. The structures and morphologies of the prepared electrodes were characterized by scanning electron microscopy (SEM), Fourier-transformed infrared spectroscopy (FTIR), and thermogravimetric analysis (TGA) measurements; and the electrochemical behaviors were examined in 2 M KOH solution. SEM and FTIR characterizations reveal that activated carbon was imbedded into the polymer membrane of polyethersulfone to form a uniform and flexible hybrid membrane. When the thin polymer-carbon membrane (PCM) was used as an electrode material for supercapacitor, a high specific capacitance of 169.4 Fg^{-1} was obtained at a current density of 0.5 Ag^{-1} along with good long-term cycle life of 94.6% capacity retention after 2000 charging-discharging cycles. Benefiting from these merits, the as-fabricated PCM//PCM cell shows an excellent electrochemical property. These results suggest a promising route towards the fabrication of highly flexible electrodes for high-performance supercapacitors.

1. Introduction

With the rapid development of population and economy in the world, there is an increasingly strong demand for energy. However, traditional fossil fuels are not sustainable energy sources [1,2]. Therefore, the development of highly efficient, stable and environmentally friendly energy storage devices is essential for

* Corresponding author. State Key Laboratory of Advanced Processing and Recycling of Non-ferrous Metals, Lanzhou University of Technology, Lanzhou, 730050, PR China.
** Corresponding author.
E-mail addresses: ranfen@163.com, ranfen@lut.cn (F. Ran), shaowei@ucsc.edu (S. Chen).

http://dx.doi.org/10.1016/j.jpowsour.2016.08.047
0378-7753/

advancing the economical use of renewable energy [3,4]. Supercapacitor, also known as electrochemical capacitor, is one type of electrochemical device that can be used to store electrical energy [5,6]. In the past several decades, supercapacitors have been attracted significant attention and applied in many areas, such as portable electronics, hybrid electric vehicles, stand-by power systems, and so on [6–9], because of its high power density, good cycle stability, fast charge-discharge capability, and safe operation [10–12].

Supercapacitors can be divided into electric double-layer capacitors (EDLCs) and pseudocapacitors based on the mechanism of charge storage and discharge [13–15]. Unlike pseudocapacitors, EDLCs utilize the surface of the electrode materials for non-faradaic storage of energy [16]. Activated carbon (AC) has been widely used as EDLC electrode materials because of its unique physicochemical properties, good conductivity, and low costs [17]. Some other carbon materials, such as carbon nanotubes, carbon onions, carbon black, and graphene have also been extensively employed as electrode materials to improve the capacity [18–22].

Nowadays, with the development of portable electronic devices such as wearable electronics, mobile phones, and flexible displays [23,24], there is an intense demand for reliable power sources and high performance with excellent flexible, light-weighted and safe supercapacitors [25–27]. Therefore, there is an urgent need to develop high-performance supercapacitors based on novel, sustainable and affordable materials [28]. Recent rapid development of carbon materials has created substantial opportunities for the fabrication of high-performance flexible electrodes [29,30]. In fact, a number of reports can be found for the synthesis of flexible carbon electrode. For example, Hu and his coworkers fabricated flexible electrode using paper as a substrate where CNTs were absorbed strongly on the paper surface [31]. Zheng et al. further extended this idea to graphene-paper, with cellulose paper directly painted with multilayer graphene [32]. Recently, another promising approach for the fabrication of freestanding carbon membranes directly was also reported [33–36]. Nevertheless, these traditional preparation methods for the preparation of flexible electrodes encounter two major drawbacks that seriously impede their practical application in supercapacitors: i) nonuniformity and insufficient contact of the component materials gave rise to poor scalability, thus resulting in mechanical degradation and low supercapacitance performance; ii) complexity of electrode preparation led to high cost for device fabrication, diminishing low-cost benefits of carbon [28]. In general, the practical applications of flexible electrodes prepared via traditional method are limited due to their complicated procedures and difficulty in constructing a uniform membrane along with sufficient-contacted components, which often leads to high costs in device fabrication, mechanical degradation of electrodes and low electrochemical performance. Therefore, it is an urgent need to develop safe, simple and low-cost synthesis method to the preparation of new flexible carbon electrodes with high performance.

Herein, we introduce a novel and facile method to fabricate flexible electrode materials based on in-situ phase separation of polyethersulfone (PES). The method based on liquid-liquid phase-separation technique, which was reduced by immersion precipitation, is widely used in the fabrication of biomedical membranes [37,38]. PES was just designed as a scaffold material for its outstanding oxidative, thermal and hydrolytic stability, as well as good mechanical and easy membrane-forming ability [39,40]; and activated carbon was used as active materials for its high capacitance performance and the low-cost attribute. Electrochemical measurements in 2 M KOH aqueous solution showed high flexibility, low impedance, and long-term stability of the hybrid membrane electrode. The synthesis method exhibits great potential for the fabrication of flexible electrode materials for supercapacitors. Moreover, the method does not involve toxic chemical treatments and the procedure is carried out in water media, minimizing environmental pollution and harm to people.

2. Experimental

2.1. Chemicals

Polyethersulfone (PES, Ultrason E6020P) was obtained from BASF, Germany. Activated carbon was purchased from Shenyang Kejing Auto-instrument Co. Ltd. All other chemicals (analytical grade) were obtained from Sinopharm Chemical Reagents Co., Ltd, China, and used without further purification.

2.2. Preparation of ultrathin hybrid membrane

In a typical synthesis, PES (3.2 g) was firstly dissolved in dimethylacetamide (DMAC) under magnetic stirring and ultrasonication to obtain a clear homogeneous solution. After the bubbles in solutions were removed by vacuum degassing, AC was added and stirred for 24 h. The casting solution was prepared as membrane by spin coating at 20 °C, which was immediately immersed in a coagulation bath of deionized water at 20 °C. Then, the ultrathin hybrid polymer-carbon membrane (PCM) was transferred to a water bath for 24 h to remove the residual solvent [16]. Finally, the membranes were dried in vacuum oven at 60 °C for 24 h. The mass ratios of PES and AC were 4:3, 4:5, 4:7, 4:11, and 4:13 (*wt*: *wt*), respectively. The experimental processes of different mass ratio were repeated for three to four times.

2.3. Materials characterization

The photographs of PCMs were acquired taken using a camera (PowerShot S100V, Canon, Japan). The microstructures and morphologies were characterized by field emission scanning electron microscope (SEM, JSM-6701F, JEOL, Japan), and thermogravimetric analysis (TGA) (DSC/DTA-TG, STA 449 F3, Germany). FTIR spectra were measured with FTIR Nexus 670 instrument. The surface area was calculated using the Brunauer-Emmett-Teller (BET) equation. Pore size distribution was calculated by the Barrett-Joyner-Halenda (BJH) method using the adsorption branch of the isotherm.

2.4. Electrode preparation

For the preparation of PCM electrode, a thin membrane of about 1×1 cm^2 was cut from the membrane, and pressed between two foam nickels (Chang Sha Lyrun New Material Co. Ltd., 90 PPI, 2 mm) of 1.5×2 cm in size (the nickel foam functions as the current collector) at 10 MPa. The capacitance values were calculated based on the mass of PCM membrane. For the AC electrodes were prepared according to the method reported in the literature [41], AC powder, acetylene black, and conducting graphite at a mass ratio of 80: 7.5: 7.5 (*wt%*) was added in an agate mortar until a homogeneous black powder was obtained. To this mixture, polytetrafluoroethylene (5 *wt%*) was added with a few drops of ethanol. The resulting paste was pressed at 10 MPa to nickel foam that served as a current collector then dried at 80 °C for 12 h. Each AC electrode contained 4 mg of the electroactive material and had a geometric surface area of 1 cm^2. And the masses of PCM electrodes are 3.7, 5.1, 6.6, and 7.8 mg at the mass ratios of 4:3, 4:5, 4:7, and 4:11.

2.5. Electrochemical characterization

All electrochemical measurements were conducted in a classical

three-electrode glass cell setup at room temperature. The synthesized samples, platinum foil electrode (1.5 × 1.5 cm) and a saturated calomel electrode (SCE) served as working electrode, counter electrode and reference electrode, respectively. 2 M KOH aqueous solutions served as electrolytes in this study. The performance of electrochemical properties was tested using cyclic voltammetry (CV), galvonostatic charge-discharge (GCD) and electrochemical impedance spectroscopy (EIS) in a CHI660E (Shanghai, China) electrochemical workstation. The CVs of all samples were tested in the same voltage window (−1.0 to 0.0 V) within the range of potential scan rates from 5 to 50 mVs^{-1}. GCD was carried out from 0.5 to 5 Ag^{-1} over a voltage range of −1.0 to 0.0 V vs. SCE. Electrochemical impedance spectroscopy (EIS) was measured within a frequency range of 10.0 mHz to 10.0 kHz at the open circuit voltage of −0.5 V. The cycle stability test was carried out on a land cell tester between −1.0 to 0.0 V with 2000 times. The self-discharge experiment was carried out using CT2001A (Land, China). The capacitor was charged to 1 V at 0.5 Ag^{-1} before its open-circuit potentials were recorded with time.

3. Results and discussion

3.1. Preparation and characterization of polymer-carbon membrane (PCM)

The fabrication process of ultrathin hybrid membrane by using in-situ liquid-liquid phase separation is schematically illustrated in Scheme 1. For the fabrication of polymer membrane (PM) a clear homogeneous solution of PES was spread into membranes by spin coating technique, and immediately immersed into a coagulation bath of deionized water coupled with the phase separation process. During the phase separation process, the solvent DMAC was dissolved in the deionized water, leading to the generation of a porous structure (Scheme 1a). PCM was fabricated in the same way. The only difference was the addition of AC in the casting solution, which was mixed well under magnetic stirring. After liquid-liquid phase separation, AC was distributed in the polymer uniformly, which made the component materials in good contact with each other. The cross-section structure of PCM, as shown in Scheme 1b, was similar to that of PM. The polymer PES, used as scaffold in this method, endows the PCM with high flexibility. Note that the present approach was easy, fast and low-cost for the preparation of flexible electrode.

The morphologies and microstructures of PM, AC and PCM were examined by SEM analysis. It can be seen from Fig. 1a and b that the thickness of PM was about 80 μm and a large number of pores existed on the pore surface. The AC particles were in different sizes from 50 nm to 5 μm (Fig. 1c and d). Fig 1e and f presents the cross-section photographs of PCM at the mass ratio of 4:11. The thickness of PCM was about 80 μm according to the SEM images. Note that the thickness of PCM could be controlled readily by adjusting the concentration of the casting solution and the speed of spinning coating. There were no finger-like pores in PCM due to the high concentration of AC; however, a large number of pore structures were formed in PCM. The interconnected pores around carbon particles were formed by fast solvents exchange during the phase separation procedure, which provided an excellent passageway and a large surface area for enhanced electrode/electrolyte interfacial contact during electrochemical process [42–44]. It is very important that PES membrane embedded with AC particles in the matrix has an obvious nanoscale network structure; this helps maintain the good distribution of AC and thus provide the high flexibility of PCM electrode membrane. It can be seen from Fig. 1g and h that an ultrathin hybrid membrane electrode consisting of AC and PES was prepared. The thin and dark membrane was smooth, flat with a uniform thickness, similar to the PES membrane. The membrane showed an excellent mechanical flexibility, which can be bent over 90°. In order to investigate the difference of PCM after the pressure, the structure and morphology were characterized by SEM (Fig. 1i and j) after the preparation of PCM electrode at 10 MPa; from the figure, one can see that after the pressure (10 MPa) on the electrodes the thickness of PCM was about 60 μm, smaller to that of PCM without pressure (80 μm). However, the nanoscale network structures of the membrane changed almost nothing.

The PCM was further characterized by FTIR measurements. As shown in Fig. 2, the bands at 1577, 1485, and 1407 cm^{-1} may be ascribed to the vibrations of benzene rings; the peak at 1241 cm^{-1} can be attributed to the stretching vibrations of C—O—C. The peaks of S═O stretching vibrations at 1151 and 1106 cm^{-1} can also be recognized clearly [45]. Compared with the spectra of PES and AC,

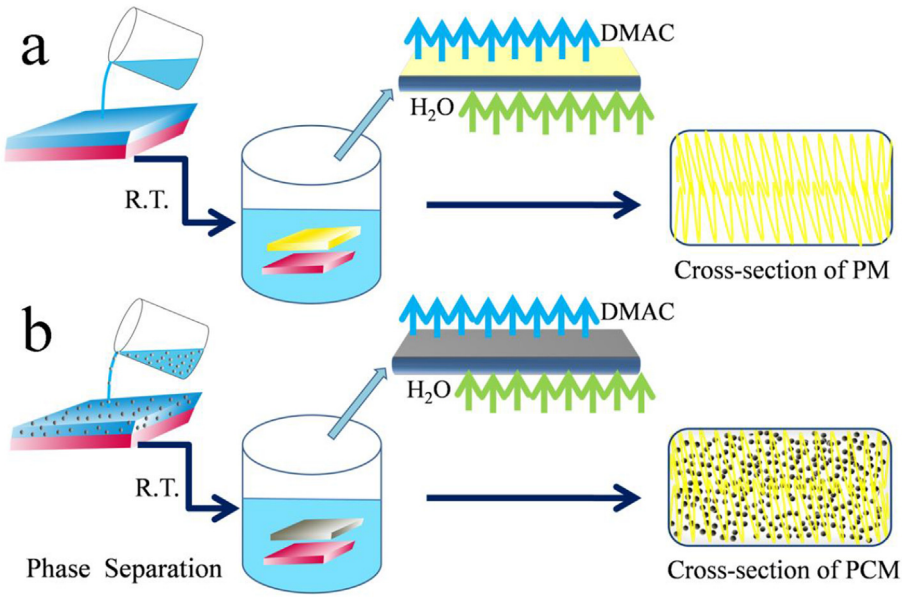

Scheme 1. Schematic illustration of PM (a) and PCM (b) fabrication processes.

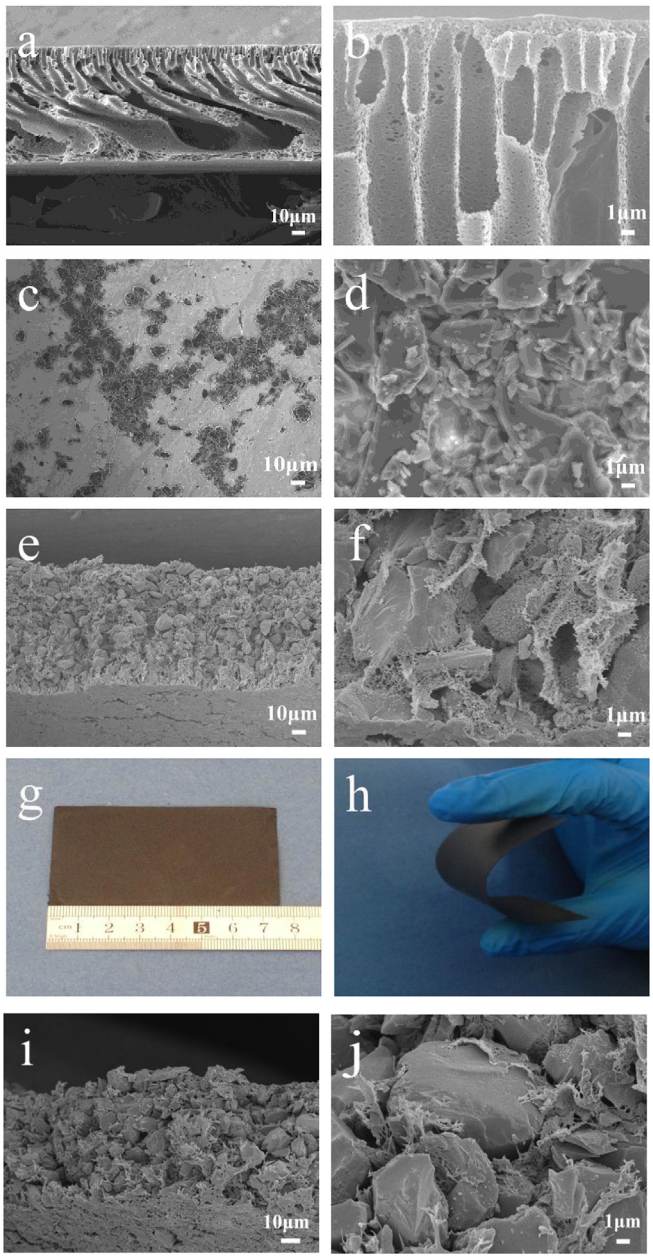

Fig. 1. Photographs and SEM images of PM and PCM. a) and b) are the cross-section views of PM; c) and d) are the AC; e) and f) are the cross-section views of PCM; and g) and h) are the overviews of PCM (4:11, *wt*: *wt*); i) and j) are the cross-section views of PCM (4:11, *wt: wt*) after a pressure of 10 MPa.

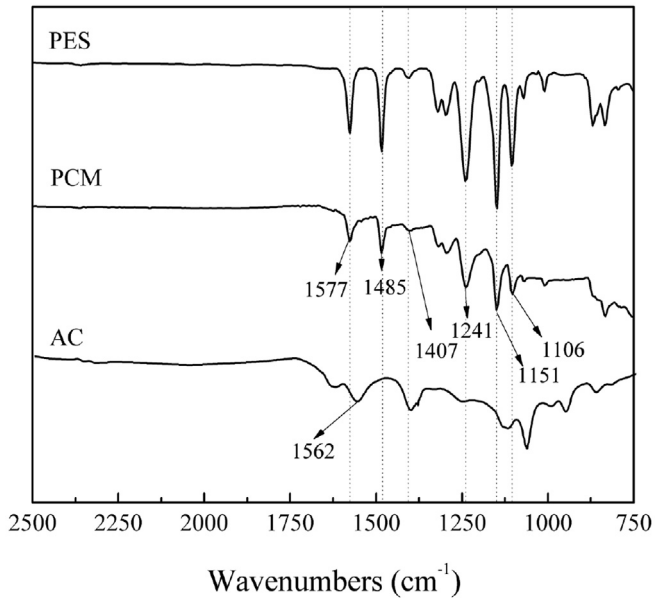

Fig. 2. FTIR spectra of PES, AC and PCM (4: 11, *wt*: *wt*).

no new functional groups were generated. The adsorption of AC lead to a band in 1562 cm^{-1}, characteristic of the stretching vibration of C=C. This indicates that PES and AC were the only components of the PCM, which were bonded strongly due to the in-situ preparation method.

In order to further investigate the thermal stability of the hybrid composite of PCM, TGA analysis was carried out under a nitrogen atmosphere. From Fig. 3a, it can be found that the mass loss of PCM occurred around 140–300 °C, which can be ascribed to the removal of the non-carbon component in activated carbon. This is consistent with the TGA results of AC, which contains 80–90 *wt%* of carbon, and 10–20 *wt%* of blends, such as oxygen, hydrogen, and ash [46,47]. The activated carbon used in this paper is one kind of commercial carbons and used without further purification. Besides, the PCM showed a weight loss of about 12 *wt%* from 450 °C, which can be ascribed to the decomposition of PES. Compared with pure PES and AC, the contents of AC in composite were close to the expected value based on the initial feeding ratio. And the mechanical properties of PES and the PCM composites were studied using tensile-strain test. From Fig. 3b, it can be found that the tensile strength and Young's modulus of pristine PES membrane were 2.90 and 71.6 MPa, respectively; while the corresponding values for the PCM were lower, i.e., 1.36 and 63.3 MPa, respectively. This indicates that the use of the PES considerably improved the mechanical properties of the PCM composites. And the prepared PCM composites have certainly mechanical capacity to be used as flexible supercapacitor materials.

The thin membrane electrode, consisting of AC and PES, was successfully prepared with the mass ratio varied from 4:3 to 4:11 (*wt*: *wt*). The photographs and SEM images of PCMs prepared at different mass ratio of PES and AC are shown in Fig. 4. It can be seen from the figure that all the prepared PCMs were smooth and flat, similar to PM. The thicknesses of PCMs were 60–90 μm. With the increase of the mass ratio, the finger-like pores in PCMs gradually disappeared and the color of PCMs became darker, which indicate that more AC particles were adhered to the PCMs prepared with a large amount of AC in the membrane. However, the flexibility of PCM varies gradually due to the AC addition. When the mass ratio reached 4:13 (*wt*: *wt*), the membrane was somewhat breakable and did not show any flexibility (Fig. 4m). Of these, the thin membrane with the mass ratio of 4:11 (*wt*: *wt*) having high flexibility was preferred and selected as the best proportion.

The porous structure was further characterized by Nitrogen adsorption-desorption curves (Fig. 5). From nitrogen adsorption-desorption isotherms, the sample exhibited type-IV isotherms [48]. The N_2 uptake at pressures of P/P0 < 0.2 indicates the relative volume of the micropores. And the N_2 uptake at the middle relative pressure proves the existence of mesopores. Pore size distributions were further calculated by the BJH method using the adsorption branch of the isotherm. The pore size distributions of PCM show a large range from 1.5 to 160 nm. BET measurements further prove the carbon material possess a structural feature including micropores, mesopores and macropores. The BET surface area (S_{BET}) of PCM was 625.67 m^3g^{-1}, indicating a fair porosity.

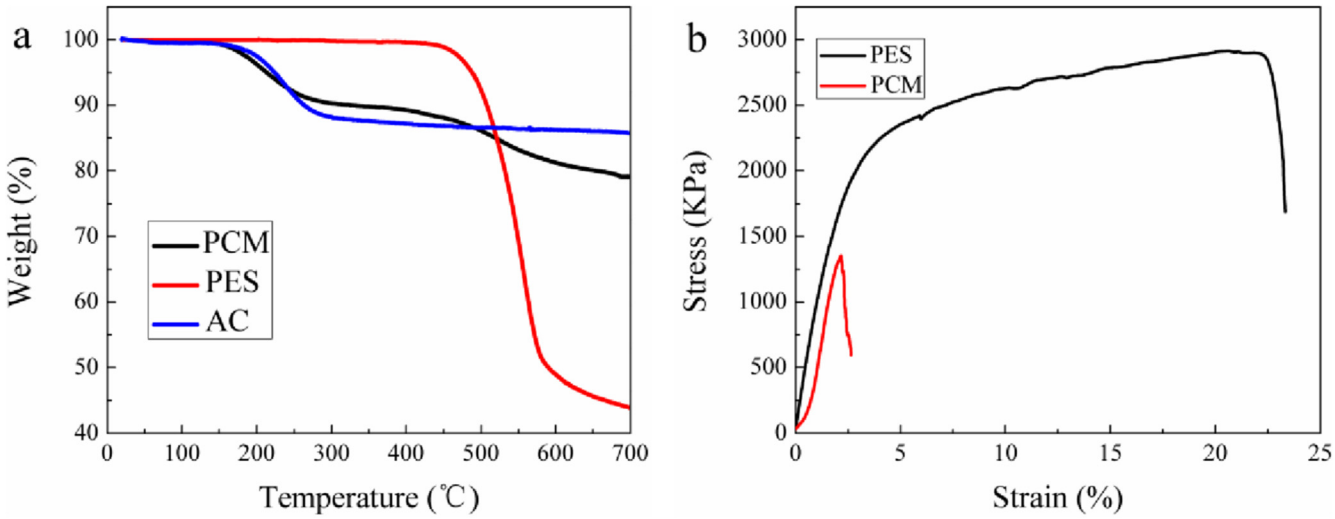

Fig. 3. (a) TGA curves of PES, AC and PCM (4:11, *wt*: *wt*) under a nitrogen atmosphere; and mechanical properties (b) of PCM (4:11, *wt*: *wt*) and PES.

3.2. Electrochemical behavior of PCM

Fig. 6 shows the CV and the galvanostatic charging-discharging curves of PCM (4:11, *wt*: *wt*) and the pristine AC electrodes obtained in 2 M KOH aqueous solution in a three-electrode system. The CV curves of PCM showed an approximate typical electrical double layer capacitive behavior (Fig. 6a). At a low scan rate, the sweep curves were symmetric on the positive and negative sweeps; the quasi-rectangular shapes demonstrated its electrical double layer capacitive behavior [49]. When the scan rate increased from 5 to 10 mVs^{-1}, the shape deviated from that of a typical electrical double layer capacitive. The distortion in the CV curves at high scan rate is due to the limited diffusion and migration of electrolyte ions in the bulk of materials. This is a common disadvantage of carbon monoliths. The galvanostatic charging-discharging curves (Fig. 6b) showed a typical triangular shape. Especially, at a high current density, the charging and discharging curves were symmetric, confirming that PCM can be one kind of excellent membrane materials for supercapacitor electrode. That is to say, the CV curves displaying a relatively rectangular shape and the galvanostatic charging-discharging curves showing a typical triangular shape indicate that the PCM electrode had a typical capacitive behavior and good charging–discharging reversibility, which further confirmed that the PCM electrode exhibited a similar electrochemical performance of AC (Fig. 6c and d).

The specific capacitances were also calculated from galvanostatic charging-discharging curves according to the following equation:

$$C_m = C/m = I\Delta t/m\Delta V \quad (1)$$

Where C_m (Fg^{-1}) is the specific capacitance, I (A) is discharge current, Δt (s) is the discharge time, ΔV (V) represents the potential drop during discharge process, and m (g) is the mass of the active material [50,51]. The specific capacitance values of PCMs were 169.4, 149.6, 139.9, 134.2, 130.8, and 128.2 Fg^{-1} at the current densities of 0.5, 1.0, 2.0, 3.0, 4.0, and 5.0 Ag^{-1}, respectively. The capacitance remains 75.7% when the discharge current increased from 0.5 to 5 Ag^{-1}. And for the AC electrode, the specific capacitance values were 243.5, 202.0, 172.9, 159.2, 148.4, and 140.8 Fg^{-1} at the same current densities with PCM. The capacitance remained 57.8%, less than the PCM electrodes. The specific capacitance values of PCMs were a little smaller than AC; it can be attributed to the adding of PES, which is one kind of non-conductive polymers and results to an increasing resistance. The capacitance values were calculated based on the mass of PCM membrane (including the mass of AC and PES). Meanwhile, the high rate capability of PCM owns to the supporting role of PES, which makes the structures of PCM more stable in the testing process. Furthermore, as a control, a spin-coated composite film at the same mass ratio of 4: 11 was prepared. And the capacitance performance is lower than that of PCM (4: 11, *wt*: *wt*) (Fig. S2). The specific capacitance values of spin-coated film were 159.5, 135.7, 123.7, 118.5, 115.4, and 112.7 Fg^{-1} at the current densities of 0.5, 1.0, 2.0, 3.0, 4.0, and 5.0 Ag^{-1}, respectively. The capacitance remains 70.7% when the discharge current increased from 0.5 to 5 Ag^{-1}. More important, the spin-coated film was fragile and owned a poor flexibility (Fig. S1). So, in this work we conducted the experiment depending on the phase-separation process.

The electrochemical behaviors of PCMs at different AC/PCM mass ratios were also examined using 2 M KOH aqueous solution as electrolyte in a three-electrode system, as shown in Fig. 7. The CV curves of PCMs at different mass ratios at a scan rate of 50 mVs^{-1} displayed a similar quasi-rectangular shape within the potential window of −1.0 to 0.0 V vs. *SCE*, revealing its electrical double layer capacitive behavior (Fig. 7a). All galvanostatic charging-discharging curves tested at a current density of 0.5 Ag^{-1} showed a typical triangular shape (Fig. 7b). The calculated specific capacitances of PCMs were 24.0, 97.8, 116.8, and 169.4 Fg^{-1} at the mass ratios of 4:3, 4:5, 4:7, and 4:11, respectively. And the detailed specific capacitance values of PHMs in different mass ratios at different current densities were also displayed (Fig. 8f). With the increase of current density, the specific capacitances of PHMs showed a slight decline, but the specific capacitance of PHM (4:11, *wt*: *wt*) exhibited the highest values than others at the different current densities.

Electrochemical impedance spectroscopy (EIS) tests were then carried out over a frequency range of 10.0 kHz to 10.0 mHz (Fig. 7c). All the impedance curves were similar, composed of one semicircle at high frequency followed by a linear component at low frequency. The semi-circle indicates the charge-transfer resistance and the vertical line demonstrates good energy storage behavior. The diameters of the semicircles for PCMs were bigger than that of AC, but the values were overall small, indicating that the small charge-transfer resistance of PCM. Note that the diameter of the semicircle for PCM (4:3, *wt*: *wt*) was bigger than the others; and this can be attributed to the large mass ratio of PES, which was adverse to

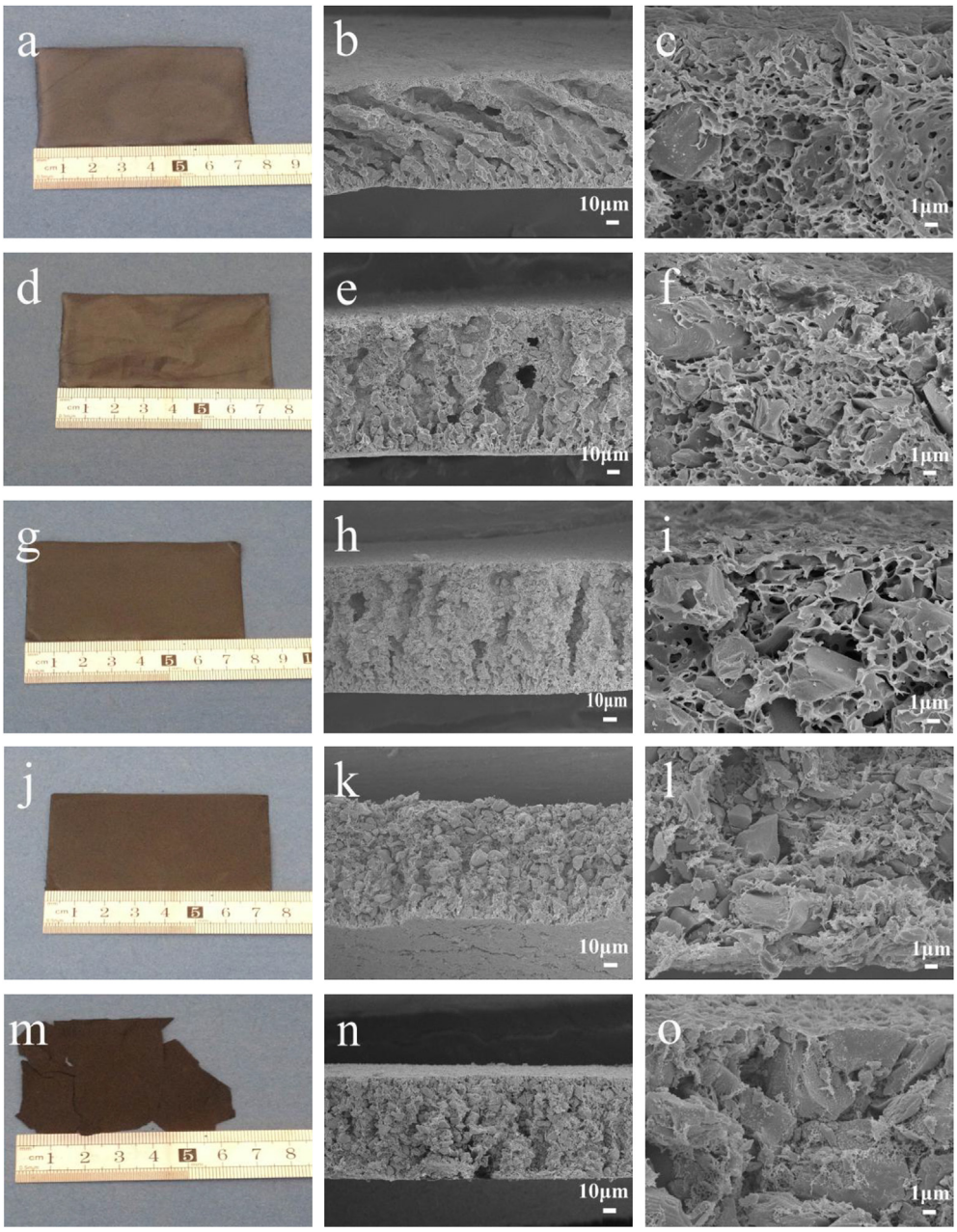

Fig. 4. Photos and SEM images of cross-section view of PCMs prepared in different mass ratios. a), b) and c) 4:3; d), e) and f) 4:5; g), h) and i) 4:7; j), k), and l) 4:11; and m), n) and o) 4:13 (*wt*: *wt*).

charge transfer. In addition, these plots showed a Warburg angle higher than 45°, indicating the suitability of the PCM as the electrode materials for supercapacitors. Besides, the internal resistances of PCMs electrodes, obtained from the intercept of the plots on real axis, are very similar (1.20, 1.35, 1.25, and 1.25 Ω, respectively). The specific capacitances of PCMs in different mass ratios at a current density of 0.5 Ag^{-1} are shown in Fig. 7d. From the data, one can see that the PCM (4:11, *wt*: *wt*) sample exhibits a highest capacitance of about 169.4 Fg^{-1}. In view of the high flexibility and the low-cost property of PCM, this capacitance value was remarkable for carbon-based supercapacitors. Moreover, the electrical conductivities of PCMs in different mass ratios were further characterized using four-point probe technique (Fig. S3). According to the histogram, the PCM (4:11, *wt*: *wt*) exhibited a larger value than other films. The electrical conductivity of PCM (4:11, *wt*: *wt*) was 0.288 S/m, showing the best conductivity.

Cyclic stability is another important property for supercapacitors. The cyclic stability of PCM (4:11, *wt*: *wt*) electrode was further examined by galvanostatic charging-discharging over 2000 cycles at a discharge current density of 1 Ag^{-1} within the voltage range −1.0 to 0.0 V *vs*. SCE, as shown in Fig. S4. The PCM electrode exhibited an excellent long life along with 94.6% specific capacitance retained after 2000 cycle tests, which indicates its excellent cycle stability and a very high degree of reversibility in the repetitive charging-discharging cycling. From the charging-discharging curves in the middle of the picture, it also can be found that the PCM electrode keep an excellent process of charging-discharging, demonstrating its stable cycling performances. This perfect performance can be attributed to the excellent cycle-to-cycle stability and good conductivity of AC. The electrical conductivity and

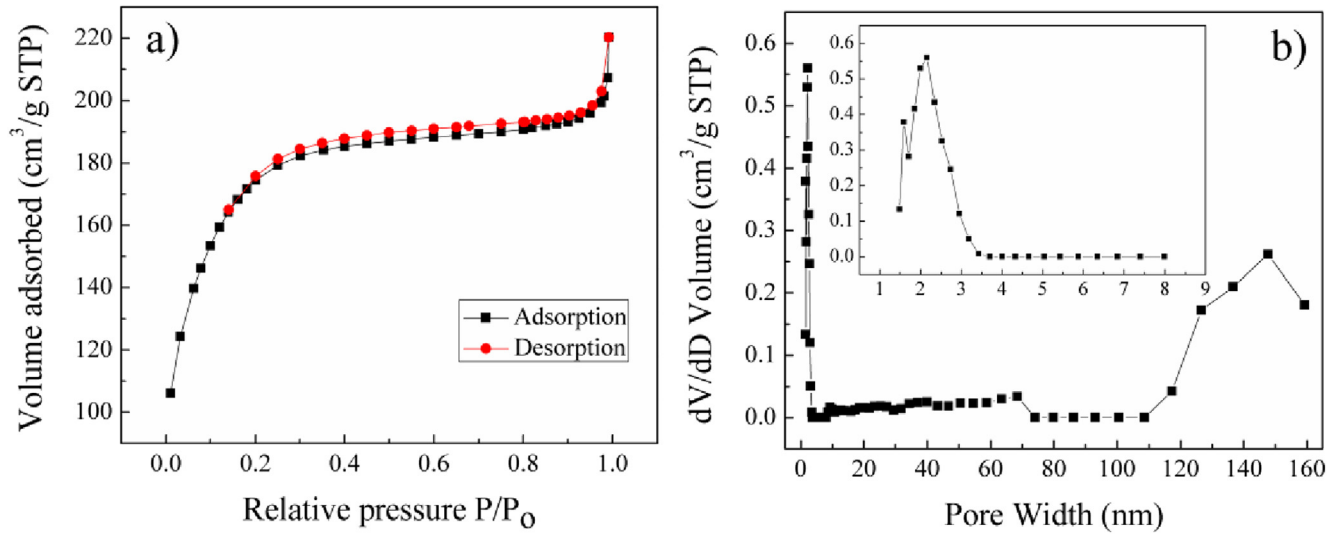

Fig. 5. (a) Nitrogen adsorption-desorption isotherms and (b) corresponding pore size distributions of PCM (4:11, *wt: wt*).

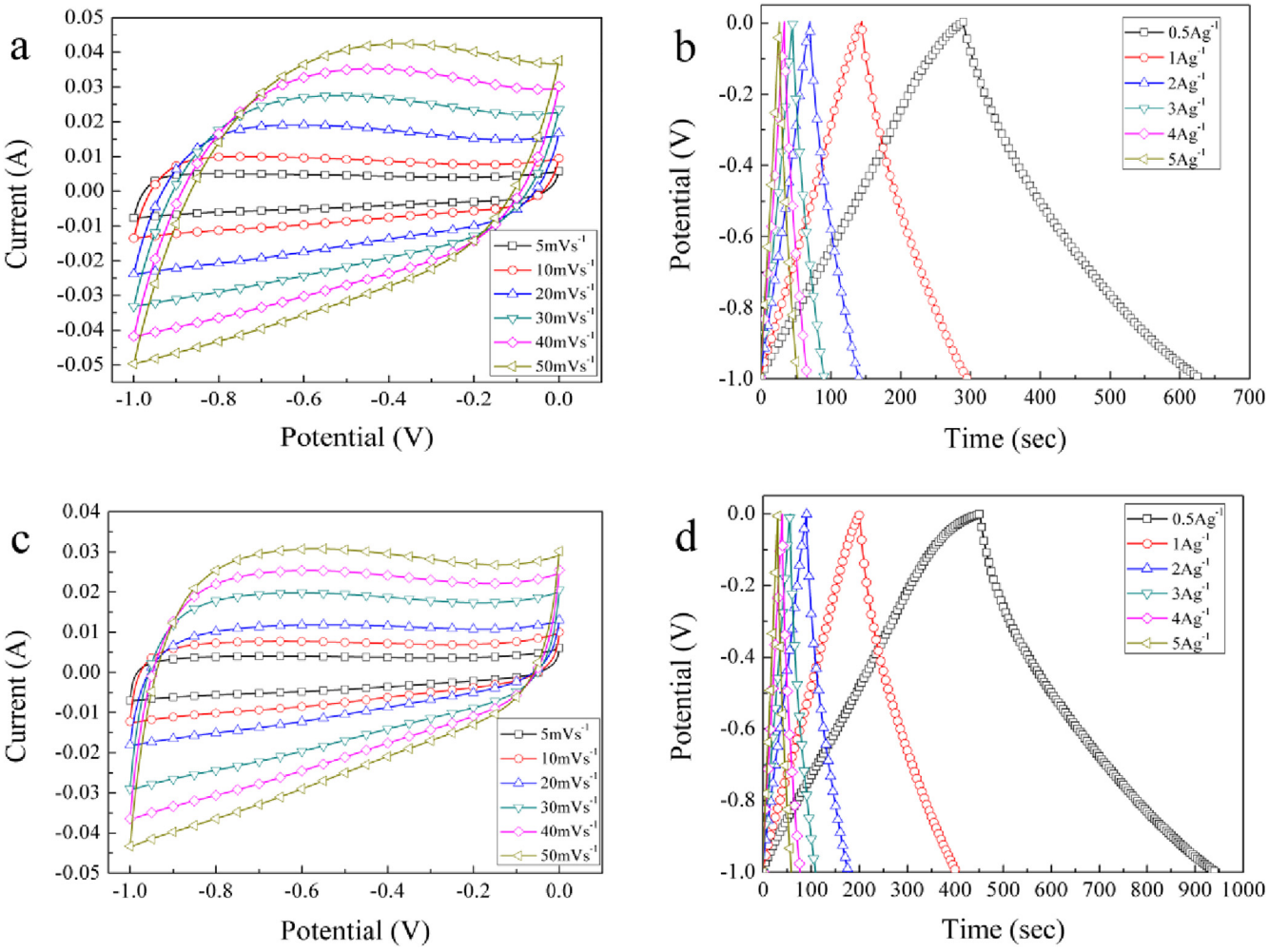

Fig. 6. Cyclic voltammogram curves of PCM (4:11, *wt*: *wt*) (a) and AC (c) at different scan rates over a potential range from −1.0 to 0 V; and galvanostatic charging-discharging curves of PCM (4:11, *wt*: *wt*) (b) and AC (d) at different current densities in 2 M KOH aqueous solution.

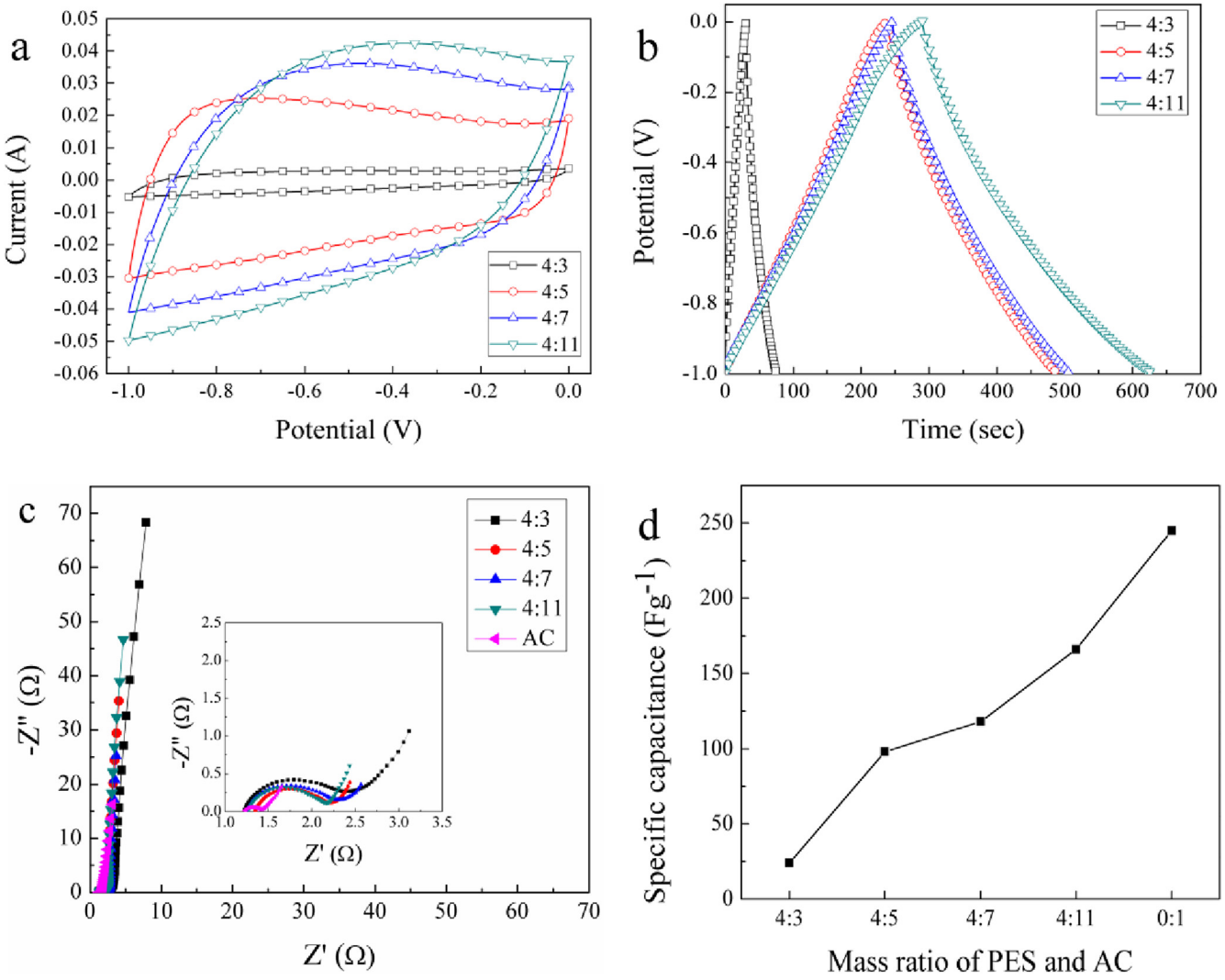

Fig. 7. Cyclic voltammogram at scan rate of 50 mVs^{-1} (a); galvanostatic charging-discharging at current density of 0.5 Ag^{-1} (b); electrochemical impedance spectroscopy curves (c); and line chart of specific capacitance at current density of 0.5 Ag^{-1} in different mass ratios of 4:3, 4:5, 4:7, 4:11 (*wt*: *wt*) and pure AC, respectively (d).

electrochemical impedance spectroscopy were further tested after the cycling (Fig. S5), and both of them had almost no change in value, indicating an excellent stability.

3.3. Symmetric supercapacitors

Based on the AC/PES composite, the SC was fabricated in a 2 M KOH aqueous electrolyte. To obtain an advanced supercapacitor, balancing the charges stored at the positive electrode (Q_+) and the negative electrode (Q_-), the optimal mass ratio between positive and negative electrodes was expected to be 1:1. The CV curves for the PCM//PCM SC at different scan rates in the potential range of 0–1.0 V (Fig. 8a) exhibit nearly symmetrical rectangular shapes, indicative of a typical capacitive behavior. The galvanostatic charging-discharging curves of the symmetric supercapacitor at different current densities are shown in Fig. 8b. It can be seen that both charging and discharging curves remain a good symmetry, similar to the result of CV curves. And no obvious IR drop was observed in each discharge curves, implying the low internal resistance of the SC. The specific capacitance values of the SC were calculated from the discharging curves based on the total mass of the two electrodes. The specific capacitance reached a maximum of 24.1 Fg^{-1} at 0.5 Ag^{-1} and still retained 16.4 Fg^{-1} at a high current density of 5 Ag^{-1} (a full charging-discharging within 7 s), the detailed specific capacitances at different densities were also shown in Fig. 8f. Furthermore, the long-term cycling stability of SC was examined by charging-discharging cycling at a current density of 1 Ag^{-1} (Fig. 8c), after 2000 cycles, the capacitance retention of SC is 62.5%, and the coulombic efficiency of SC retained the nearby of 98%, demonstrating the SC keeps a good electrochemical reversibility. The low specific capacitance and the poor capacity retention can be ascribed to the higher resistance of PCMs. On the one side, the resistance of the electrode increased because of the addition of PES in the electrode. On the other side, when the PCM//PCM cell was fabricated using two similar PCMs, the resistance of the cell further increased compared to that of the pristine AC. But the high flexibility of the device would be promising especially after the possible modification and improvement on the stability of PCM during the future studies. Fig. 8d shows the self-discharge behavior of SC. Compared to the pristine AC, PCM composite had a little faster discharge rate. After 3600 s, the potential of PCM retained 0.31, and that of the AC electrode showed 0.43. This result can be attributed to the adding of PES. The initial fast potential drop is due to a diffusion process of ionic species near the electrode surface

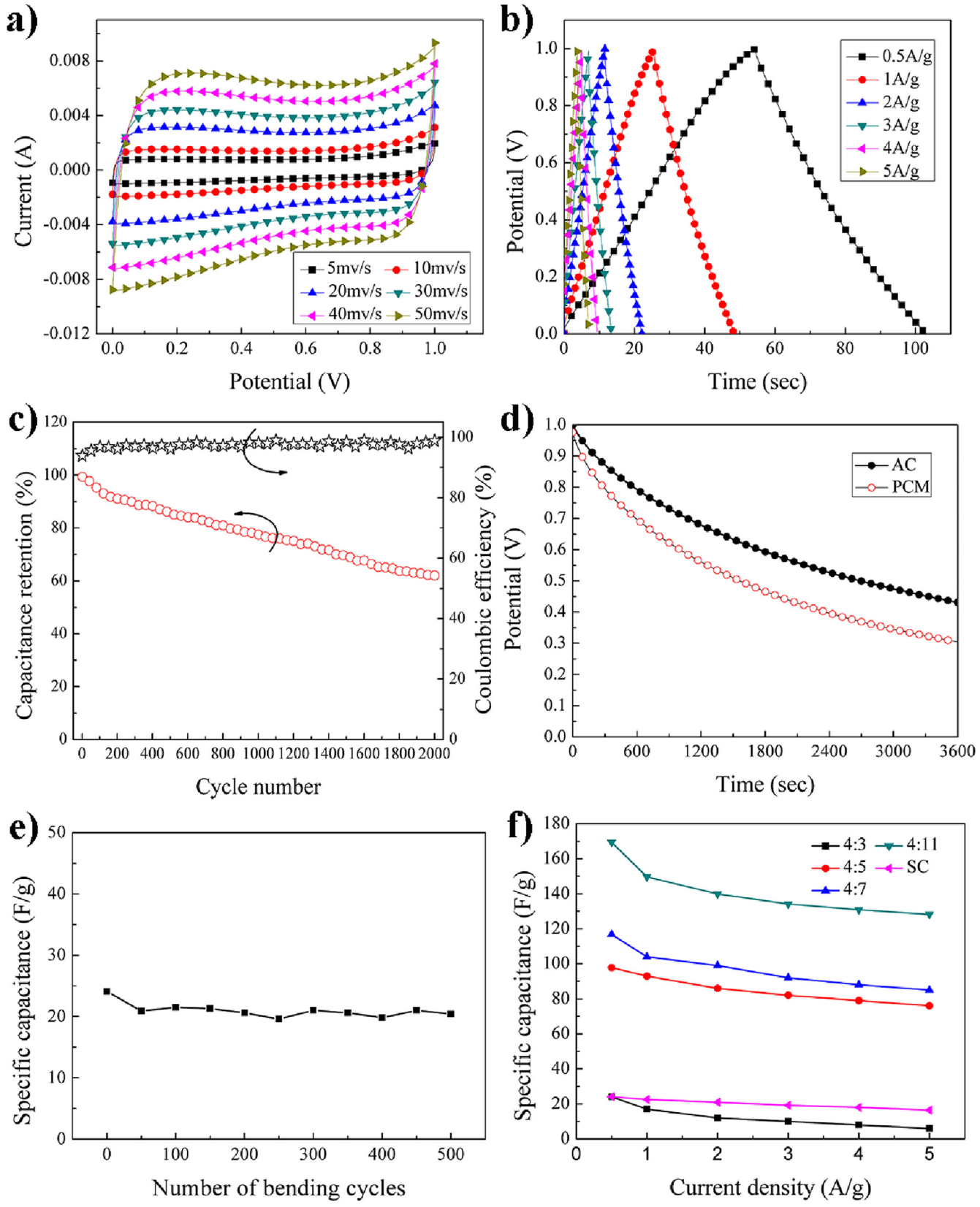

Fig. 8. (a) Cyclic voltammograms, (b) galvanostatic charging-discharging curves, (c) cycle life and coulombic efficiency, (d) self-discharge of PCM in 2 M KOH solution, (e) The specific capacitance of flexible PCM//PCM SC tested at a current density of 1 A/g versus bending cycles, (f) the specific capacitances of PCMs prepared in different mass ratios and SC at different current densities.

during charging [52]. Meanwhile, the flexibility of the device was further tested by repeated bending to 180° for 500 cycles, and only a small fluctuation in capacitance was observed (Fig. 8e). In addition, a flexible device was set up using the PCM, and showed great flexibility (Video 1). It can be bent to 180° and did not show detectable changes from the original state when flattened after bending (Fig. S6).

Supplementary video related to this article can be found at http://dx.doi.org/10.1016/j.jpowsour.2016.08.047.

4. Conclusions

In summary, an ultrathin hybrid membrane of polymer-carbon membrane PES/AC (PCM) was fabricated by in-situ liquid-liquid phase separation method, which exhibits excellent flexibility and high electrochemical behaviors, such as low resistance, good cyclic stability, and high specific capacitance. The PCM prepared at the PES/AC ratio of 4:11 (*wt*:*wt*) presented a specific capacitance of 169.4 Fg^{-1} at the current density of 0.5 Ag^{-1} in 2 M KOH solution; and after 2000 charging-discharging cycles, 94.6% of the specific capacitance was retented. And the PCM//PCM symmetric supercapacitor showed excellent double-layer electrochemical behaviors. Furthermore, the fabrication strategy was easy, safe and low-cost, providing an applicable route to develop flexible electrode materials.

Acknowledgements

This work was partly supported by the National Natural Science Foundation of China (51203071, 51363014 and 51362018), China Postdoctoral Science Foundation (2014M552509, 2015T81064), the Program for Hongliu Distinguished Young Scholars in Lanzhou University of Technology (J201402), and the University Scientific Research Project of Gansu Province (2014B-025). Natural Science Funds of the Gansu Province (2015GS05123).

Appendix A. Supplementary data

Supplementary data related to this article can be found at http://dx.doi.org/10.1016/j.jpowsour.2016.08.047.

References

[1] J.P. Holdren, Energy and sustainability, Science 315 (2007), 737–737.
[2] V.S. Arunachalam, E.L. Fleischer, The global energy landscape and materials innovation, Mrs Bull. 33 (2008) 264–276.
[3] R. Cao, Z.L. Yang, Energy storage technologies in renewable energy electricity generation system, Mater. Sci. Eng. Technol. (2012) 462.
[4] L.H. Yang, Z. Xu, J. Ostergaard, Hopf bifurcation and eigenvalue sensitivity analysis of doubly fed induction generator wind turbine system, in: Power and Energy Society General Meeting IEEE, 2010, pp. 1–6.
[5] B.E. Conway, Electrochemical Supercapacitors: Scientific Fundamentals and Technological Application, Kluwer Academic/Plenum Publishers, New York, 1999.
[6] P. Simon, Y. Gogotsi, Materials for electrochemical capacitors, Nat. Mater. 7 (2008) 845–854.
[7] J.R. Miller, P. Simon, Materials science: electrochemical capacitors for energy management, Sci. Mag. 321 (2008) 651–652.
[8] F. Su, C.K. Poh, J.S. Chen, G. Xu, D. Wang, Q. Li, Nitrogen-containing microporous carbon nanospheres with improved capacitive properties, Energy Environ. Sci. 4 (2011) 717–724.
[9] Y. Zhai, Y. Dou, D. Zhao, P.F. Fulvio, R.T. Mayes, S. Dai, Carbon materials for chemical capacitive energy storage, Adv. Mater. 23 (2011) 4828–4850.
[10] B. Andrew, Ultracapacitors: why, how, and where is the technology, J. Power Sources 91 (2000) 37–50.
[11] X.S. Zhang, L.L. Zhao, Carbon-based materials as supercapacitor electrodes, Chem. Soc. Rev. 38 (2009) 2520–2531.
[12] S.W. Lee, B.M. Gallant, H.R. Byon, P.T. Hammond, S.H. Yang, Nanostructured carbon-based electrodes: bridging the gap between thin-film lithium-ion batteries and electrochemical capacitors, Energy Environ. Sci. 4 (2011) 1972–1985.
[13] L.Z. Fan, Y.S. Hu, J. Maier, P. Adelhelm, B. Smarsly, M. Antonietti, High electroactivity of polyaniline in supercapacitors by using a hierarchically porous carbon monolith as a support, Adv. Funct. Mater. 17 (2007) 3083–3087.
[14] E. Frackowiak, F. Beguin, Electrochemical storage of energy in carbon nanotubes and nanostructured carbons, Carbon 40 (2002) 1775–1787.
[15] W. Wei, X. Cui, W. Chen, D.G. Ivey, Manganese oxide-based materials as electrochemical supercapacitor electrodes, Chem. Soc. Rev. 40 (2011) 1697–1721.
[16] H.L. Fan, F. Ran, X.X. Zhang, H.M. Song, W.X. Jing, K.W. Shen, Easy fabrication and high electrochemical capacitive performance of hierarchical porous carbon by a method combining liquid-liquid phase separation and pyrolysis process, Electrochim. Acta 138 (2014) 367–375.
[17] D.W. Wang, F. Li, M. Liu, G.Q. Lu, H.M. Cheng, 3D aperiodic hierarchical porous graphitic carbon material for high-rate electrochemical capacitive energy storage, Angew. Chem. Int. Ed. 47 (2008) 373–376.
[18] C. Portet, G. Yushin, Y. Gogotsi, Electrochemical performance of carbon onions, nanodiamonds, carbon black and multiwalled nanotubes in electrical double layer capacitors, Carbon 45 (2007) 2511–2518.
[19] D. Pech, M. Brunet, H. Durou, P. Huang, V. Mochalin, Y. Gogotsi, Ultrahigh-power micrometre-sized supercapacitors based on onion-like carbon, Nat. Nanotechnol. 5 (2010) 651–654.
[20] L. Dai, D.W. Chang, J.B. Baek, W. Lu, Carbon nanomaterials for advanced energy conversion and storage, Small 8 (2012) 1130–1166.
[21] F. Du, D. Yu, L. Dai, S. Ganguli, V. Varshney, A.K. Roy, Preparation of tunable 3D pillared carbon nanotube-graphene networks for high-performance capacitance, Chem. Mater. 23 (2011) 4810–4816.
[22] H.J. Choi, S.M. Jung, J.M. Seo, D.W. Chang, L. Dai, J.B. Baek, Graphene for energy conversion and storage in fuel cells and supercapacitors, Nano Energy 1 (2012) 534–551.
[23] B.D. Gates, Materials science. Flexible electronics, Science 323 (2009) 1566–1567.
[24] S. Park, M. Vosguerichian, Z.A. Bao, A review of fabrication and applications of carbon nanotube film-based flexible electronics, Nanoscale 5 (2013) 1727–1752.
[25] S. Kim, H.J. Kwon, S. Lee, H. Shim, Y. Chun, W. Choi, J. Kwack, D. Han, M. Song, S. Kim, S. Mohammadi, I. Kee, S.Y. Lee, Low-Power flexible organic light-emitting diode display device, Adv. Mater. 23 (2011) 3511–3516.
[26] M. Koo, K.I. Park, S.H. Lee, M. Suh, D.Y. Jeon, J.W. Choi, K. Kang, K.J. Lee, Bendable inorganic thin-film battery for fully flexible electronic systems, Nano Lett. 12 (2012) 4810–4816.
[27] S. Shi, C. Xu, C. Yang, J. Li, H.D. Du, B.H. Li, F.Y. Kang, Flexible supercapacitors, Particuology 11 (2012) 371–377.
[28] Q. Zheng, Z. Cai, Z. Ma, S. Gong, Cellulose nanofibril/reduced graphene oxide/carbon nanotube hybrid aerogels for highly flexible and all-solid-state supercapacitors, ACS Appl. Mater. Interfaces 7 (2015) 3263–3271.
[29] Y. Cheng, J. Liu, Carbon nanomaterials for flexible energy storage, Mater. Res. Lett. 1 (2013) 175–192.
[30] K. Jost, C.R. Perez, J.K. McDonough, V. Presser, M. Heon, G. Dion, Y. Gogotsi, Carbon coated textiles for flexible energy storage, Energy Environ. Sci. 4 (2011) 5060–5067.
[31] L. Hu, H. Wu, Y. Cui, Printed energy storage devices by integration of electrodes and separators into single sheets of paper, Appl. Phys. Lett. 96 (2010) 183502–183503.
[32] G. Zheng, L. Hu, H. Wu, X. Xie, Y. Cui, Paper supercapacitors by a solvent-free drawing method, Energy Environ. Sci. 4 (2011) 3368–3373.
[33] Y.M. He, W.J. Chen, X.D. Li, Z.X. Zhang, J.C. Fu, C.H. Zhao, E.Q. Xie, Freestanding three-dimensional graphene/MnO_2 composite networks as ultralight and flexible supercapacitor electrodes, ACS Nano 7 (2013) 174–182.
[34] H. Gwon, H.S. Kim, K.U. Lee, D.H. Seo, Y.C. Park, Y.S. Lee, B.T. Ahn, K. Kang, Flexible energy storage devices based on graphene paper, Energy Environ. Sci. 4 (2011) 1277–1283.
[35] H. Gao, F. Xiao, C.B. Ching, H. Duan, Flexible all-solid-state asymmetric supercapacitors based on free-standing carbon nanotube/graphene and Mn_3O_4 nanoparticle/graphene paper electrodes, ACS Appl. Mater. Interfaces 4 (2012) 7019–7025.
[36] K.Z. Gao, Z.Q. Shao, J. Li, X. Wang, X.Q. Peng, W.J. Wang, F.J. Wang, Cellulose nanofiber–graphene all solid-state flexible supercapacitors, J. Mater. Chem. A 1 (2013) 63–67.
[37] H.M. Song, F. Ran, H.L. Fan, X.Q. Niu, L. Kang, C.S. Zhao, Hemocompatibility and ultrafiltration performance of surface-functionalized polyethersulfone membrane by blending comb-like amphiphilic block copolymer, J. Membr. Sci. 471 (2014) 319–327.
[38] F. Ran, X.Q. Niu, H.M. Song, C. Cheng, W.F. Zhao, S.Q. Nie, L.G. Wang, A.M. Yang, S.D. Sun, C.S. Zhao, H.M. Song, H.M. Song, Toward a highly hemocompatible membrane for blood purification via a physical blend of miscible comb-like amphiphilic copolymers, Biomater. Sci. 2 (2014) 538–547.
[39] F. Ran, S.Q. Nie, W.F. Zhao, J. Li, B.H. Su, S.D. Sun, C.S. Zhao, Biocompatibility of modified polyethersulfone membranes by blending an amphiphilic triblock co-polymer of poly(vinyl pyrrolidone)–b–poly(methyl methacrylate)–b–poly(vinyl pyrrolidone), Acta Biomater. 7 (2011) 3370–3381.
[40] C.S. Zhao, J.M. Xue, F. Ran, S.D. Sun, Modification of polyethersulfone membranes – a review of methods, Prog. Mater. Sci. 58 (2013) 76–150.
[41] J.W. Lang, X.B. Yan, W.W. Liu, R.T. Wang, Q.J. Xue, Influence of nitric acid modification of ordered mesoporous carbon materials on their capacitive performances in different aqueous electrolytes, J. Power Sources 204 (2012)

220–229.
[42] S. Kang, J.S. Yu, M. Kruk, M. Jaroniec, Synthesis of an ordered macroporous carbon with 62 nm spherical pores that exhibit unique gas absorptionproperties, Chem. Commun. 16 (2002) 1670–1671.
[43] Z. Lei, Y. Zhang, H. Wang, Y. Ke, J. Li, F. Li, J. Xing, Fabrication of well-ordered macroporous active carbon with a microporous framework, J. Mater. Chem. 11 (2001) 1975–1977.
[44] K.W. Shen, F. Ran, Y.T. Tan, X.Q. Niu, H.L. Fan, K. Yan, L.B. Kong, L. Kang, Toward interconnected hierarchical porous structure via chemical depositing organic nano-polyaniline on inorganic carbon scaffold for supercapacitor, Synth. Met. 199 (2015) 205–213.
[45] H.W. Tang, L.P. Zhang, S. Li, G.J. Zhao, Z. Qiu, S.Q. Sun, Study on spectroscopic characterization and property of PES/micro-nano cellulose composite membrane material, Spectrosc. Spectr. Anal. 30 (2010) 630–634.
[46] B.K. Pradhan, N.K. Sandle, Effect of different oxidizing agent treatments on the surface properties of activated carbons, Carbon 37 (1999) 1323–1332.
[47] A. Bagreev, H. Rahman, T.J. Bandosz, Thermal regeneration of a spent activated carbon previously used as hydrogen sulfide adsorbent, Carbon 39 (2001) 1319–1326.
[48] Y. Meng, D. Gu, F. Zhang, Y. Shi, L. Cheng, D. Feng, A family of highly ordered mesoporous polymer resin and carbon structures from organic self-assembly, Chem. Mater. 18 (2006) 4447–4464.
[49] Y. Jiang, X.T. Ling, Z. Jiao, L. Li, Q.L. Ma, M.H. Wu, Y.L. Chu, B. Zhao, Flexible of multiwalled carbon nanotubes/manganese dioxide nanoflake textiles for high-performance electrochemical capacitors, Electrochim. Acta 153 (2015) 246–253.
[50] Y.T. Tan, F. Ran, L.B. Kong, Polyaniline nanoparticles grown on the surface of carbon microspheres aggregations for electrochemical supercapacitors, Synth. Met. 162 (2012) 114–118.
[51] M.C. Liu, L.B. Kong, C. Lu, X.M. Li, Y.C. Luo, L. Kang, A Sol-gel process for the synthesis of NiCo2O4 having improved specific capacitance and cycle stability for electrochemical capacitors, J. Electrochem. Soc. 159 (2012) A1262–A1266.
[52] J. Hu, H.L. Wang, X. Huang, Improved electrochemical performance of hierarchical porous carbon/polyaniline composites, Electrochim. Acta 74 (2012) 98–104.